Mutations in Citron Kinase Cause Recessive Microlissencephaly with Multinucleated Neurons

Mutations in *Citron-Kinase* cause recessive micro-lissencephaly with multinucleated neurons.

Harding B[1, 11], Moccia A[2, 11], Soukarieh O[3], Tubeuf H[3], Drunat S [4,5], Chitty L[6], Verloes A [4,5], Gressens P [5,7,8], El Ghouzzi V [5], Joriot S [9], Passemard S [4,5,7], Di Cunto F [10], Martins A[3], Bielas S. L.[2]*

[1]Pathology and Laboratory Medicine, Perelman School of Medicine, University of Pennsylvania and Children's Hospital of Philadelphia, Philadelphia, Pennsylvania, U.S.A. 19104

[2] Department of Human Genetics, University of Michigan Medical School, Ann Arbor, Michigan, U.S.A. 48109

[3]Inserm-U1079-IRIB, University of Rouen, Normandy Univ, Normandy Centre for Genomic and Personalized Medicine & Interactive Biosoftware, Rouen, France 76183

[4] Département de Génétique, Hôpital Robert Debré, Paris, France 75019

[5] Inserm U1141, Protect, Hôpital Robert Debré, Paris, France 75019

[6] Genetics and Genomic Medicine, UCL Institute of Child Health and Great Ormond Street NHS Foundation Trust, London, U.K. WC1N 1EH

[7] Université Paris Diderot, Hôpital Robert Debré, Paris, France 75019

[8] Center for Developing Brain, King's college, St Thomas' Campus, London, United Kingdom WC2R 2LS

[9] Service de Neuropédiatrie, Centre Hospitalier Régional Universitaire de Lille, Lille, France 59037

[10] Department of Molecular Biotechnology and Health Sciences, University of Turin, Italy 10126

[11] These authors contributed equally to this work

*Corresponding Author

Stephanie L. Bielas, Department of Human Genetics, University of Michigan Medical School, 3703 Medical Science II, 1137 Catherine St. SPC 5618, Ann Arbor, MI 48109-5618, U.S.A.
Phone: 001.734.647.8890; Fax: 001.734.763.3784; E-mail: sbielas@umich.edu.

Conflict of interest: The authors have declared that no conflict of interest exists.

Keywords: Cytokinesis, Neurogenesis, Primary Microcephaly, Lissencephaly, Autosomal Recessive, Citron Kinase, Splicing Mutation.

Abstract:

Primary microcephaly is a neurodevelopmental disorder caused by a reduction in brain size attributed to defects in proliferation of neural progenitor cells during development. Mutations in genes encoding proteins that localize to the mitotic spindle and centrosomes have been implicated in the pathogenicity of primary microcephaly. In contrast, the contractile ring and midbody required for cytokinesis, the final stage of mitosis have not previously been implicated in the molecular mechanisms of this phenotype. Citron Kinase (CIT) is a multi-domain protein that localizes to the cleavage furrow and midbody of mitotic cells, where it is required for the completion of cytokinesis. Rodent models of *Cit* deficiency highlighted the role of this gene in neurogenesis and microcephaly over a decade ago. Here we identify recessively inherited pathogenic variants in *CIT* as the genetic basis of severe microcephaly and neonatal death. We present postmortem data showing that CIT is critical to build a normally sized human brain. Consistent with cytokinesis defects attributed to CIT, multinucleated neurons are observed throughout the cerebral cortex and cerebellum of an affected proband, expanding our understanding of mechanisms attributed to primary microcephaly.

Main:

Primary microcephaly is a genetically heterogeneous neurodevelopmental disorder characterized by a severe reduction in brain growth [1]. This decreased brain volume often stems from a primary defect in neurogenesis. The cerebral cortex is composed of neurons born from neural progenitor cells (NPCs) that reside adjacent to the lateral ventricle during early neurodevelopment [2]. The mitotic machinery of NPCs is critical for rapid expansion of the progenitor pool underlying normal brain growth and maintenance of neural progenitor multipotency. Based largely on human genetics findings, primary microcephaly has been largely attributed to defects in the fidelity of mitotic spindle placement and centrosome stability [3-8]. Surprisingly, other steps in mitosis have not been implicated by neurogenetics in the pathophysiology of microcephaly, despite a series of rodent models showing that cleavage furrow placement, constriction of the contractile ring and abscission by the midbody are critical for neurogenesis [9-11].

CIT is a multi-domain protein that localizes to the cleavage furrow and midbody where it functions in cytokinesis, the final steps of mitosis (Fig. 1A) [12,13]. CIT has a N-terminal kinase domain and a number of C-terminal domains that facilitate interactions between contractile ring components (anillin, actin, myosin and RhoA). While the endogenous substrates of CIT have yet to be confirmed, experimental data from multiple organisms shown that the kinase activity and scaffolding functions of Cit are both important for successful completion of cytokinesis [12,14,15]. Conversely, neurons with two or more fully-formed nuclei can result from incomplete cytokinesis. The impact of cytokinesis defects on brain development and size are evident in the *Cit* knockout mouse and the *Flathead* rat with a spontaneous nonsense mutation in *Cit* exon 1. In rodents, Cit is critical for proliferation of NPCs and male germ cell precursors. *Cit* null animals are characterized by microcephaly, testicular hypoplasia, ataxia, growth deficiencies and lethal epilepsy [10,11]. These phenotypes have been linked to cytokinesis defects and the presence of

multinucleated cells throughout the cortex and cerebellum. Premature differentiation of early NPCs and widespread apoptosis accumulate across development, resulting in a cerebral cortex and cerebellum less than 50% the size of normal brain. Cortical hypoplasia and layer disorganization are predicted to account for the recurrent spontaneous seizures and premature death in the mice [16]. Roles for *CIT* [MIM 605629] in human brain development and primary microcephaly have been predicted but not yet reported.

Here we describe three independent families (A, B and C), each with multiple affected children who presented with severe micro-lissencephaly associated with neonatal mortality (Fig. 1B). The clinical features of the probands are provided in Table 1. Egyptian Family A is consanguineous with two microcephalic male siblings. The first affected child died in the neonatal period (Fig. 1B). Proband A was delivered at term and weighed 2600 grams (2 SD below the age/sex mean) consistent with the 5th percentile for growth. Head circumference, not measured until 3.5 months of age, was 27cm (11 to 12 SD below the age/sex mean). His length at 3.5 months was 53 cm (4 to 5 SD below the age/sex mean), and he continued to experience failure to thrive thereafter. Dysmorphisms were noted including hypotelorism, sloping forehead and relatively large ears (Fig. 3A). He exhibited axial hypotonia, upper and lower extremity hypertonia, increased deep tendon reflexes and lack of head support. Microcephaly was confirmed by magnetic resonance imaging (MRI), which revealed lissencephaly, enlarged ventricles, agenesis of the corpus callosum, cerebellar hypoplasia and brainstem hypoplasia (Fig. 3B). T2 hyperintensity was also noted throughout the white matter consistent with spastic tetraplegia.

Family B has two affected children born to consanguineous parents from United Arab Emirates. Male Proband B was noted to have microcephaly, intrauterine growth retardation, and oligohydramnios by ultrasound at 30 gestational weeks (GWs). Echocardiogram indicated

cardiomegaly, biventricular dilatation and tricuspid regurgitation. He was delivered by spontaneous vaginal delivery at 39 GWs with a head circumference of 24cm (8 SD below the age/sex mean) and a body length measurement of 27.2cm crown-rump (2.5 SD below the mean) consistent with 36 GWs. Despite Apgar scores of 8 at one minute, and 9 at 5 minutes, he died the following day.

At birth, the brain weight of Proband B was 40g (10% the average newborn brain weight of 390g). The cerebral hemispheres were lissencephalic and separated by shallow Sylvian fissures. Corpus callosum agenesis, large ventricles and small well-delineated basal ganglia and thalami were noted (Fig. 3C-E). The brain stem and cerebellum were hypoplastic with small cerebellar folia (Fig. 4A). Dysmorphic facial features were noted including prominent occiput, absent fontanelle, large ears, wide nasal bridge, prominent upper lip, highly arched palate, cloudy corneas, right-sided single palmar crease and hypoplastic nails. Renal aplasia was also noted. This constellation of features were similar to those observed during the pregnancy and birth of a previously affected female infant from the same pedigree who presented with microcephaly and renal agenesis, and survived only 4 hours following birth (Fig. 1B).

Proband C is the first-born son of unrelated French parents, delivered at full term. His birth weight was 2900g, body length was 46cm, and had a head circumference of 30cm (1, 2 and 3.5 SD below the age/sex mean respectively) consistent with a diagnosis of microcephaly. Proband C presented with a sloping forehead, prominent nose, and relatively large ears. His neurological examination was remarkable for upper and lower limb hypertonia and brisk tendon reflexes in the lower limbs. He walked independently at 18 months of age. He has developmental delay with moderate to severe ID and mild autistic features. No metabolic, ERG or EEG abnormalities were detected. By age 10 years, his head circumference was 6.5 SD below the age/sex mean. An MRI performed at this age showed simplified gyral pattern and hypoplastic cerebellum (Fig.

4F-G). A second child in this family (II:2) was also confirmed to have microcephaly by fetal MRI at 29 GWs (Fig. 3H-I). The biparietal diameter measured from the fetal MRI at that time was consistent with 23 GWs.

Whole exome sequencing (WES) and candidate gene screening were employed to identify a genetic diagnosis for these three probands. Parents provided written informed consent that was approved by IRB committees at the respective institutions. Quad WES (mother, father, proband and unaffected sibling) was performed for Family A to empower the identification of pathogenic variants. DNA was isolated from peripheral blood using standard procedures. WES was performed at Beijing Genomics Institute (BGI) using standard protocols for Agilent SureSelect All Exon kit-v4 library preparation, Illumina HiSeq 2000 sequencing to a mean sequence depth of 98X for 99% exome coverage and the sequence was analyzed using the SOAPaligner [17,18]. Variants were filtered by dbSNP, 1000 Genomes, ESP6500 database and the BGI SNP database. An average of 65,457 high-quality single nucleotide, insertion and deletion variants (SNVs and Indels) were identified per individual. Common variants (minor allele frequency (MAF) >0.005) were removed and rare variants were analyzed relative to homozygous recessive, compound heterozygous and dominant modes of inheritance. Targeted analysis did not identify a causal mutation in any gene present in the OMIM database and was therefore followed by a complete analysis of all coding regions. A homozygous recessive G>A transition (c.1111+1G>A; g. chr12: 120,260,623, hg19), disrupting the donor splice site of exon 9 in *CIT* (NM_007174.2), was identified consistent with consanguinity (Fig. 1C). Segregation of this variant in the family was confirmed by Sanger sequencing, with both parents and the unaffected sibling being heterozygous carriers.

The potential impact on RNA splicing produced by the c.1111+1G>A nucleotide variant was first evaluated by using *in silico* approaches (Human Splicing Finder and MaxEntScan). This

analysis predicted the destruction of the reference donor site (WT 5'ss), but also revealed the presence of cryptic donor sites both upstream and downstream the reference 5' ss (Fig. 2A). We then evaluated the impact on splicing experimentally by performing a minigene reporter assay as previously described [19]. Briefly, the genomic region of interest (*CIT* exon 9 and at least 150 bp of flanking intronic sequences) was amplified from genomic DNA both from a control individual and from Proband A (*CIT* c.1111+1G>A), and then inserted into the intron of the pCAS2 reporter plasmid in order to generate 3-exon WT and Mut minigenes, respectively. Next, the plasmids were transfected into HeLa cells, RNA extracted 24 h post-transfection and the splicing pattern of the minigenes assessed by RT-PCR and sequencing of the gel-purified RT-PCR products [20]. Our results confirmed that the c.1111+1G>A variant results in the production of aberrantly spliced transcripts due to the concomitant destruction of the reference 5'ss and activation of two cryptic 5'ss located nearby. As shown in Figures 2B and 2C, and in Figure S1, the major aberrant transcripts induced by c.1111+1G>A result from the activation of a cryptic 5'ss located downstream the reference 5'ss, leading to the aberrant retention of the first 4 nt from intron 9 in the minigene's transcripts. In the context of *CIT* transcripts, this alteration is expected to produce a frameshift resulting in the introduction of a premature termination codon in exon 10, potentially targeting the aberrant transcripts to degradation by nonsense mediated decay. The minor aberrant transcripts induced by c.1111+1G>A result from the activation of a cryptic 5'ss located upstream the reference 5'ss, leading to the aberrant deletion of 54 nt from exon 9 in the minigene's transcripts. In the context of *CIT* transcripts, this alteration is expected to produce an in-frame deletion resulting in the production of a protein lacking 18 amino acids in the kinase domain of CIT (CIT^{-18aa}). The stability of mutant CIT^{-18aa} has not been evaluated, but it is possible that the deletion disrupts kinase activity.

Resequencing of *CIT* coding exons and splice junctions in 35 additional probands with primary microcephaly identified two additional individuals, Probands B and C, with recessive pathogenic variants. Proband B DNA was extracted from formalin-fixed, paraffin-embedded brain tissue using Qiagen QIAamp DNA FFPE Tissue Kit (Catalog Number 56404) per the manufacturer's instructions. The 46 coding exons of *CIT* on chromosome 12 were screened by dideoxy sequence analysis on an ABI 3730 sequencer (Applied Biosystems, Life Technologies), and sequence traces were analyzed with Sequencher 5.1 (Gene Codes Corporation). A homozygous pathogenic mutation consistent with consanguinity was identified in Proband B. This 10bp deletion in exon 2 of *CIT*, creates a premature stop codon after 15 codons downstream (NM_007174.2; c.29_38delATCCTTTGGA; g.chr12:120,313,935-120,313,944 hg19; p.Asn10Metfs*15) and is predicted to function as a null allele (Fig. 1A,D). The non-neural phenotypes observed in Proband B may represent the human-specific tissues that are sensitive to homozygous truncating variants in *CIT* (Table S2). Likewise, the syndromic features and neonatally mortality of these cases are not suggestive of a diagnosis of autosomal recessive primary microcephaly (MCPH).

Proband C and Subject C:II:2 DNA was isolated from peripheral blood using standard procedures at the Robert Debré Hospital, Paris. *CIT* was included on a microcephaly gene panel for cohort screening by RainDance microdroplet PCR and 2X150bp sequencing with Illumina MiSeq. Deep sequencing (142X) reads were mapped to hg19 with MiSeq analysis software and BWA-GATK, and panel exons were 99% covered. Variants were filtered against MAF (>0.005), dbSNP, 1000 Genomes, Exome Variant Server and an in-house dataset. Rare variants were annotated for functional features of coding nucleotides with publically available databases outlined for WES. Both Proband C and Subject C:II:2 were found to carry compound heterozygous *CIT* variants located in the kinase domain; one generating a nonsense variant in exon 4 (c.412C>T; g. chr.12: 120,295,329 hg19; p.Gln138*) and the other generating a

missense variant in exon 5 (c.473C>G; g. chr12: 120,288,021 hg19; p.Pro158Arg) (Fig. 1A,F). As shown in Figure S1, none of these new *CIT* variants (c.29_38delATCCTTTGGA, c.412C>T, and c.473C>G) had an impact on RNA splicing. The p.Pro158Arg variant is predicted to disrupt kinase function, but not CIT expression. The stable expression of the p.Pro158Arg variant might ameliorate the severity of the microcephaly exhibited in this individual, as compared with the homozygous null phenotypes in Probands A and B. The parents and unaffected relatives in Families B and C were not available for carrier testing.

The *CIT* mutations presented here were absent from online genomic variant databases, including the 1000 Genomes Project, National Heart, Lung and Blood Institute (NHLBI) ESP6500, dbSNP 141, and the Exome Aggregation Consortium (ExAC) [21-23]. Bioinformatic variant annotation using SeattleSeq Variation Annotation revealed that the point mutations in our probands affect highly conserved bases with high GERP and CADD scores that are predicted to be pathogenic (Table 1) [24,25]. Further analysis of the genetic variation in *CIT* showed that loss-of-function alleles are infrequent. Homozygous nonsense or frameshift variants were not present in the ExAC browser. However, fifteen rare heterozygous truncating variants were detected (MAF <0.001), suggesting there is high evolutionary pressure against these alleles and supporting the deleteriousness of the recessive *CIT* variants described here. These findings correspond to a Residual Variation Intolerance Score (RVIS) of -2.35 indicating CIT is in the top 1.14% of genes in the genome intolerant to common functional genetic variation [26].

The cytokinesis functions of CIT have been conserved across evolution. Deficiencies of Cit have been shown to disrupt NPC proliferation, implicating CIT in primary microcephaly. While severe reductions in brain size are often accompanied by a simplified gyral pattern, it is mutations in genes that disrupt neuronal migration that are generally attributed to classical lissencephaly, or

228 smooth brain disorders[1,27-29]. This combination of extreme reduction of brain volume and
229 lissencephaly observed in Probands A and B may provide evidence for a reduction of cortical
230 surface area that does not support gyri formation in the human brain. This idea is supported by
231 the genotypic-phenotypic spectrum of micro-lissencephaly based on recessive inheritance of
232 *CIT* pathogenic variants, described here and in an accompanying study. Homozygous missense
233 variants in the kinase domain of *CIT* are associated with primary microcephaly with a simplified
234 gyral pattern and few additional syndromic features. Conversely, homozygous null variants in
235 *CIT* represent the severe end of the spectrum associated with extremely small lissencephalic
236 brains and neonatal mortality.
237
238 Given the well established role for CIT in cytokinesis, our three cases provide evidence that this
239 is an important pathogenic mechanism for microcephaly, a disorder previously linked primarily
240 to gene products that localize to the centrosome or mitotic spindle [30]. This cell biology was
241 originally implicated by Aspm [MIM 605481], which localizes to the midbody where it can be co-
242 immunoprecipitated with Cit [31-33]. Severe microcephaly with widespread multinucleated neurons
243 is characteristic of the structural and cellular pathology observed in the *Cit* knockout mouse and
244 the *Flathead* rat (Table S2) [10,11]. In accordance with institutional research board and ethics
245 committee approval, post-mortem analysis of Proband B allowed the human cell and molecular
246 neuropathology associated with pathogenic variants in *CIT* to be analyzed. All non-neural
247 tissue examined had normal cytology, but multinucleated neurons were observed throughout
248 the neuraxis of Proband B, a hallmark of cytokinesis defects (Table S3). This neural specific
249 phenotype is phenocopied in the rodent models, yet the molecular details that underlie the
250 tissue specificity of this feature have not been determined.
251
252 To analyze the cytoarchitechture, Proband B brain sections were stained with H&E, while
253 selected sections were stained with Kluver-Barrera or calbindin. Microscopically, the profoundly

microcephalic cerebral cortex showed both cytological and organizational abnormalities in many areas. The neocortex was excessively thick, with the six cortical layers replaced by a molecular layer and two broad layers comprised of loosely and irregularly scattered neurons (Fig. 3J,K). The underlying white matter was unmyelinated and contained scattered ectopic neurons. The overlying leptomeninges were greatly thickened with reticulin and collagen fibers, prominently vascularized, and contained heterotopic astrocytes and neurons, some of which were multinucleated (Fig. 2L). The hippocampi were dysplastic, small and under-rotated, with hypoplastic dentate gyri (Fig. 3M-O). Based on analysis of rodent models, incomplete cytokinesis has been linked to premature differentiation of NPCs, possibly due to aberrant allocation of apically localized fate determinants in multipotent NPCs. These premature postmitotic neurons may contribute to cortical lamination defects. Alternatively, while migration defects have not been described in association with *Cit* mutations, defective radial migration of bi-nucleate immature neurons is a novel explanation of this phenotype that has not been tested.

Cortical hypoplasia and layer disorganization account for the recurrent spontaneous seizures associated with premature death in rodent models [16]. Extrapolating from these rodent models, the cytoarchitectural abnormalities observed in Proband B are consistent with cytokinesis defects that contribute to a reduced neuronal precursor proliferation, multinucleation of neurons and increased cell death. Despite the anatomical phenotypic similarities, pathogenic *CIT* variants have not been detected in epilepsy cohorts, including the Epi4K exome sequence collection of 264 epileptic encephalopathy trios [34].

The cerebellar cortex of Proband B was hypoplastic and dysplastic (Fig. 4). Laminar disorganization was more evident in the hemispheres than the vermis, where folia were fused and Purkinje cells were observed in multilayered islands interspersed by abnormal granule cell domains (Fig. 4B-H). At birth, the external granule cell layer (EGL) is usually compact, with 4-6

rows of bipolar cells abutting the molecular layer (ML) (Fig. 4B,D,G). In Proband B the EGL was wider, the ML narrower, and both were merged with the Purkinje cell layer (Fig. 4G-H). In this case the EGL was comprised of 2 or 3 compact rows of cells overlying a looser band of horizontally oriented, thin, elongated cell bodies, some clearly binucleate (Fig. 4E,F,H). Purkinje cells had short simplified dendritic arborization compared to controls and many were multinucleated (Fig. 4G-J). Likewise, the internal granular layer (IGL) was severely hypo-cellular (Fig. 4G-H).

In summary, we report the identification of pathogenic variants in *CIT* as a genetic basis for primary microcephaly and cerebellar hypoplasia, with phenotypic features remarkably similar to *Cit*$^{-/-}$ rodent models. These findings highlight the evolutionarily conserved function of CIT in neurodevelopment and the disproportionate sensitivity of the neuraxis to pathogenic variants in this gene. Multinucleated neurons are rarely observed in the nervous system, apart from their occurrence in ganglion cell tumors. These genetic findings implicate novel mechanisms in the pathogenesis of primary microcephaly and allow us to describe the human presentation of this striking multinucleated neuronal phenotype.

Acknowledgements

We thank the families for their participation and contribution to this research. We appreciate Ritesh KC and Brian McGrath for stimulating discussion during manuscript preparation, and Dr. Joseph Loturco, Dr. Joseph Gleeson, Dr. Ozgur Rosti and Dr. Hongda Li for collaborations on *CIT* genetics and molecular biology. This work was supported by the National Institutes of Health (R00HD069624 to S.L.B), the French *Institut National du Cancer/Direction Générale de l'Offre de Soins* (INCa/DGOS AAP/CFB/CI to A.M), the French Ministry of Education (PhD fellowship to O.S.) and the French National Association for Research and Technology (ANRT) in the context of public-private partnership between Inserm and Interactive Biosoftware (CIFRE

PhD fellowship to H.T.). The sponsors of the study had no role in study design, data collection, analysis and interpretation, or writing of the manuscript.

Web Resources

OMIM, (http://www.omim.org/)

UCSC Genome Browser, (http://genome.ucsc.edu)

1000 Genomes Project, (http://browser.1000genomes.org)

NHLBI Exome Sequencing Project (ESP) Exome Variant Server, (http://evs.gs.washington.edu/EVS/),

dbSNP 141, (http://www.ncbi.nlm.nih.gov/projects/SNP/)

Exome Aggregation Consortium (ExAC), (http://exac.broadinstitute.org/)

SeattleSeq Variation Annotation, (http://snp.gs.washington.edu/SeattleSeqAnnotation138/)

Residual Variation Intolerance Score (RVIS), (http://genic-intolerance.org)

World Health Organization Child Growth Standards, (http://www.who.int/childgrowth/standards/en/)

References

1. Gilmore, E.C. & Walsh, C.A. Genetic causes of microcephaly and lessons for neuronal development. *Wiley Interdiscip Rev Dev Biol* **2**, 461-78 (2013).
2. Paridaen, J.T. & Huttner, W.B. Neurogenesis during development of the vertebrate central nervous system. *EMBO Rep* **15**, 351-64 (2014).
3. Bond, J. *et al.* ASPM is a major determinant of cerebral cortical size. *Nat Genet* **32**, 316-20 (2002).
4. Bond, J. *et al.* A centrosomal mechanism involving CDK5RAP2 and CENPJ controls brain size. *Nat Genet* **37**, 353-5 (2005).
5. Kumar, A., Girimaji, S.C., Duvvari, M.R. & Blanton, S.H. Mutations in STIL, encoding a pericentriolar and centrosomal protein, cause primary microcephaly. *Am J Hum Genet* **84**, 286-90 (2009).
6. Bilgüvar, K. *et al.* Whole-exome sequencing identifies recessive WDR62 mutations in severe brain malformations. *Nature* **467**, 207-10 (2010).
7. Guernsey, D.L. *et al.* Mutations in centrosomal protein CEP152 in primary microcephaly families linked to MCPH4. *Am J Hum Genet* **87**, 40-51 (2010).
8. Nicholas, A.K. *et al.* WDR62 is associated with the spindle pole and is mutated in human microcephaly. *Nat Genet* **42**, 1010-4 (2010).
9. Gauthier-Fisher, A. *et al.* Lfc and Tctex-1 regulate the genesis of neurons from cortical precursor cells. *Nat Neurosci* **12**, 735-44 (2009).
10. Sarkisian, M.R., Li, W., Di Cunto, F., D'Mello, S.R. & LoTurco, J.J. Citron-kinase, a protein essential to cytokinesis in neuronal progenitors, is deleted in the flathead mutant rat. *J Neurosci* **22**, RC217 (2002).
11. Di Cunto, F. *et al.* Defective neurogenesis in citron kinase knockout mice by altered cytokinesis and massive apoptosis. *Neuron* **28**, 115-27 (2000).

12. El Amine, N., Kechad, A., Jananji, S. & Hickson, G.R. Opposing actions of septins and Sticky on Anillin promote the transition from contractile to midbody ring. *J Cell Biol* **203**, 487-504 (2013).
13. Green, R.A., Paluch, E. & Oegema, K. Cytokinesis in animal cells. *Annu Rev Cell Dev Biol* **28**, 29-58 (2012).
14. Gai, M. *et al.* Citron kinase controls abscission through RhoA and anillin. *Mol Biol Cell* **22**, 3768-78 (2011).
15. Bassi, Z.I. *et al.* Sticky/Citron kinase maintains proper RhoA localization at the cleavage site during cytokinesis. *J Cell Biol* **195**, 595-603 (2011).
16. Ackman, J.B., Ramos, R.L., Sarkisian, M.R. & Loturco, J.J. Citron kinase is required for postnatal neurogenesis in the hippocampus. *Dev Neurosci* **29**, 113-23 (2007).
17. Li, R. *et al.* SNP detection for massively parallel whole-genome resequencing. *Genome Res* **19**, 1124-32 (2009).
18. Li, R. *et al.* SOAP2: an improved ultrafast tool for short read alignment. *Bioinformatics* **25**, 1966-7 (2009).
19. Soukarieh, O. *et al.* Exonic Splicing Mutations Are More Prevalent than Currently Estimated and Can Be Predicted by Using In Silico Tools. *PLoS Genet* **12**, e1005756 (2016).
20. Gaildrat, P. *et al.* Use of splicing reporter minigene assay to evaluate the effect on splicing of unclassified genetic variants. *Methods Mol Biol* **653**, 249-57 (2010).
21. Abecasis, G.R. *et al.* A map of human genome variation from population-scale sequencing. *Nature* **467**, 1061-73 (2010).
22. Psaty, B.M. *et al.* Cohorts for Heart and Aging Research in Genomic Epidemiology (CHARGE) Consortium: Design of prospective meta-analyses of genome-wide association studies from 5 cohorts. *Circ Cardiovasc Genet* **2**, 73-80 (2009).

23. Lek, M. *et al.* Analysis of protein-coding genetic variation in 60,706 humans. *bioRxiv* (2015).
24. Cooper, G.M. *et al.* Distribution and intensity of constraint in mammalian genomic sequence. *Genome Res* **15**, 901-13 (2005).
25. Kircher, M. *et al.* A general framework for estimating the relative pathogenicity of human genetic variants. *Nat Genet* **46**, 310-5 (2014).
26. Petrovski, S., Wang, Q., Heinzen, E.L., Allen, A.S. & Goldstein, D.B. Genic intolerance to functional variation and the interpretation of personal genomes. *PLoS Genet* **9**, e1003709 (2013).
27. Gleeson, J.G. *et al.* Doublecortin, a brain-specific gene mutated in human X-linked lissencephaly and double cortex syndrome, encodes a putative signaling protein. *Cell* **92**, 63-72 (1998).
28. Fry, A.E., Cushion, T.D. & Pilz, D.T. The genetics of lissencephaly. *Am J Med Genet C Semin Med Genet* **166C**, 198-210 (2014).
29. Moon, H.M. & Wynshaw-Boris, A. Cytoskeleton in action: lissencephaly, a neuronal migration disorder. *Wiley Interdiscip Rev Dev Biol* **2**, 229-45 (2013).
30. Morris-Rosendahl, D.J. & Kaindl, A.M. What next-generation sequencing (NGS) technology has enabled us to learn about primary autosomal recessive microcephaly (MCPH). *Mol Cell Probes* **29**, 271-81 (2015).
31. Paramasivam, M., Chang, Y.J. & LoTurco, J.J. ASPM and citron kinase co-localize to the midbody ring during cytokinesis. *Cell Cycle* **6**, 1605-12 (2007).
32. Pulvers, J.N. *et al.* Mutations in mouse Aspm (abnormal spindle-like microcephaly associated) cause not only microcephaly but also major defects in the germline. *Proc Natl Acad Sci U S A* **107**, 16595-600 (2010).
33. Higgins, J. *et al.* Human ASPM participates in spindle organisation, spindle orientation and cytokinesis. *BMC Cell Biol* **11**, 85 (2010).

34. Consortium, E.K. Epi4K: gene discovery in 4,000 genomes. *Epilepsia* **53**, 1457-67 (2012).

402 **Table 1. Genetic and major clinical features**
403

	Proband A	Proband B	Proband C	Subject II:2 of Family C
***CIT* variant (hg19, NM_007174.2)**	Chr12: 120,260,623 c.1111+1G>A	Chr12: 120,313,935 - 120,313,944 c.29_38delATCCTTTGGA p.Asn10Metfs*15	Chr12: 120,295,329 and Chr12: 120,288,021 c.412C>T and c.473C>G p.Gln138* and p.Pro158Arg	Chr12: 120,295,329 and Chr12: 120,288,021 c.412C>T and c.473C>G p.Gln138* and p.Pro158Arg
GERP Score	5.900	N/A	4.660 and 5.280	4.660 and 5.280
CADD Score	31.000	N/A	38.000 and 27.800	38.000 and 27.800
Gender	Male	Male	Male	Male
Gestational Length	Full Term	Full Term	Full Term	Pregnancy terminated at GW 29+2
Birth Weight	2.6 kg (-2 SD)	1.730 kg (-4 SD)	2.92 kg (-1 SD)	N/A
Birth Length	Unknown (home birth)	27.2 cm (crown-rump -2.5 SD)	46 cm (-2 SD)	N/A
Birth Head Circumference (HC)	Unknown (home birth)	24 cm (-8 SD)	30 cm (-3.5 SD)	N/A
HC at Most Recent Evaluation	27 cm (-11 to -12 SD) measured at 3.5 months	N/A	43 cm (-6.5 SD) measured at 10 years	N/A
Brain Abnormalities	MRI revealed micro-lissencephaly, agenesis of corpus callosum, cerebellar and brainstem hypoplasia, and T2 hyperintensity of the whole white matter	Autopsy revealed micro-lissencephaly, absent corpus callosum, hindbrain and cerebellum hypotrophy, cerebral cortex hypotrophy, and comparatively large ventricles. Detailed neuropathology included in the main text.	MRI revealed microcephaly, simplified gyral pattern, and hypoplastic cerebellum and brainstem.	Fetal MRI revealed a microcephaly, biparietal diameter equivalent to a fetus of 23 WG, and gyration equivalent to a fetus of 26 WG
Neurological Findings	Upper and lower extremity hypertonia, axial hypotonia, increased DTRs, and spastic tetraplegia	N/A	Upper and lower extremity hypertonia, and brisk DTRs for the lower extremities	N/A
Seizures	No	N/A	No	N/A
Intellectual Disability	Not assessed	N/A	Moderate to severe ID with mild autistic features	N/A
Development	Delayed	N/A	Delayed	N/A
Dysmorphisms	Hypotelorism, sloping forehead, and relatively large ears	Prominent occiput, absent fontanelle, large ears, wide nasal bridge, prominent upper lip, high arched palate, cloudy corneas, a right-sided sinlge palmar crease and small nails	Sloping forehead, prominent nose, and relatively large ears	N/A
Status	Unknown	Deceased; one day after birth	Alive	Terminated pregnancy

404 SD = standard deviation, N/A = not available, DTR = deep tendon reflexes, WG = weeks
405 gestation. World Health Organization Child Growth Standards were applied for weight, height
406 and head circumference.
407

Figure legends

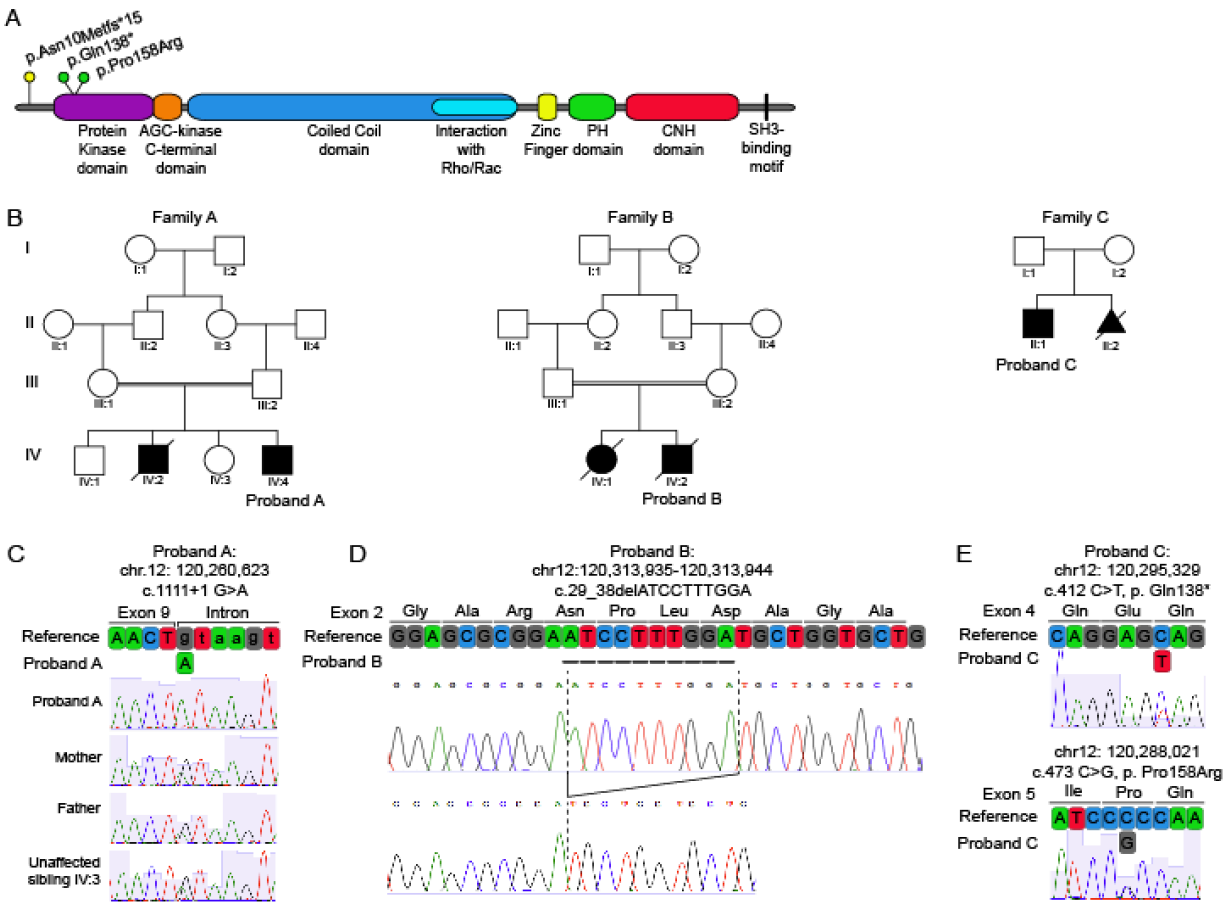

Figure 1. Recessive *CIT* variants in micro-lissencephaly. (**A**) Protein domain organization of CIT showing pathogenic coding variants relative to protein domains. (**B**) Pedigrees of the families investigated with probands noted. (**C**) Chromatographs and schematic of the WT reference *CIT* exon 9/intron 9 boundary, homozygous Proband A splice donor variant (c.1111+1 G>A) and cryptic splice donor site four bases downstream. Parents and unaffected sibling IV:3 are heterozygous carriers. (**D**) Chromatographs defining the homozygous 10 bp deletion in *CIT* exon 2 (c.29_38delATCCTTTGGA, chr12:120,313,935-120,313,944) amplified from Proband B that creates a frameshift leading to a premature stop 15 codons downstream (not shown). (**E**) Chromatographs and schematic of reference *CIT* exon 4 and exon 5 and the corresponding

nonsense (c.412C>T; p.Gln138*) and missense (c.473C>G; p.Pro158Arg) variants identified in Proband C.

Figure 2.

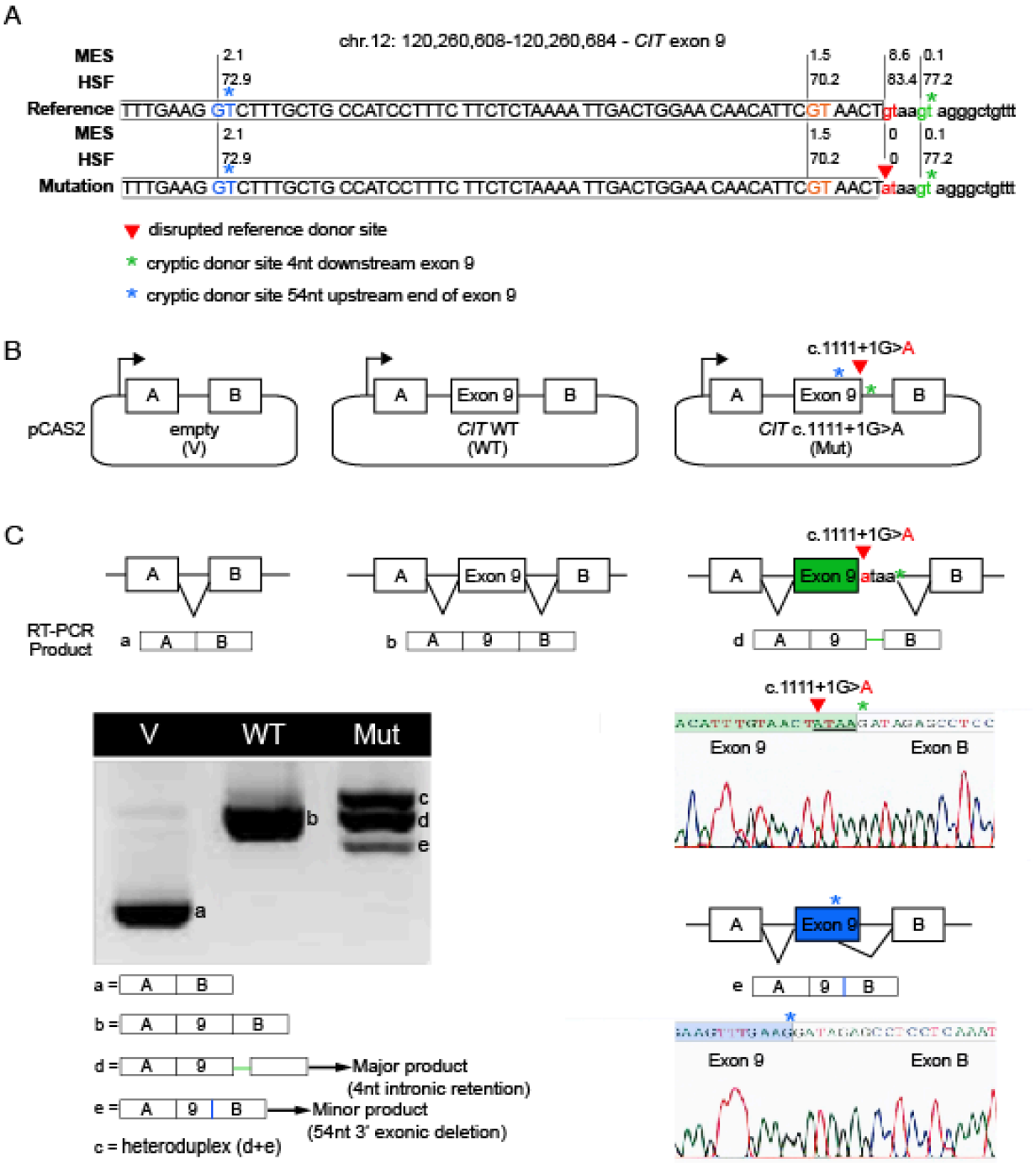

Functional analysis of *CIT* c.1111+1G>A confirms its negative impact on RNA splicing. (**A**) Schematic representation of *CIT* sequence across the exon 9-intron 9 boundary. The reference donor site (WT, red nucleotides) and cryptic donor sites (blue, orange and green nucleotides) were delineated and scored with MaxEntScan (MES) and Human Splice Finder (HSF) as shown in Figure S1. Only splice sites predicted by both algorithms in the WT sequence are shown. Exonic and intronic sequences are indicated by upper and lower case respectively. Proband A *CIT* c.1111+1 G>A substitution (red arrowhead) disrupts the WT donor site. Asterisks indicates cryptic splice sites activated in the presence of c.1111+1 G>A (**B**) A minigene splicing assay was performed as previously described [20]. Structure of the CIT-exon 9 minigenes used in the splicing reporter assay. Arrows represent the CMV promoter. Boxes represent exons and lines in-between indicate introns. (**C**) Analysis of WT and mutant (Mut) minigene splicing patterns. Transcripts were analyzed by RT-PCR after expression in Hela cells by using primers specific to minigene's exon A and B (Table S1). RT-PCR products were separated on an agarose gel and sequenced. Aberrantly spliced products are illustrated on the right with accompanying chromatographs.

Figure 3.

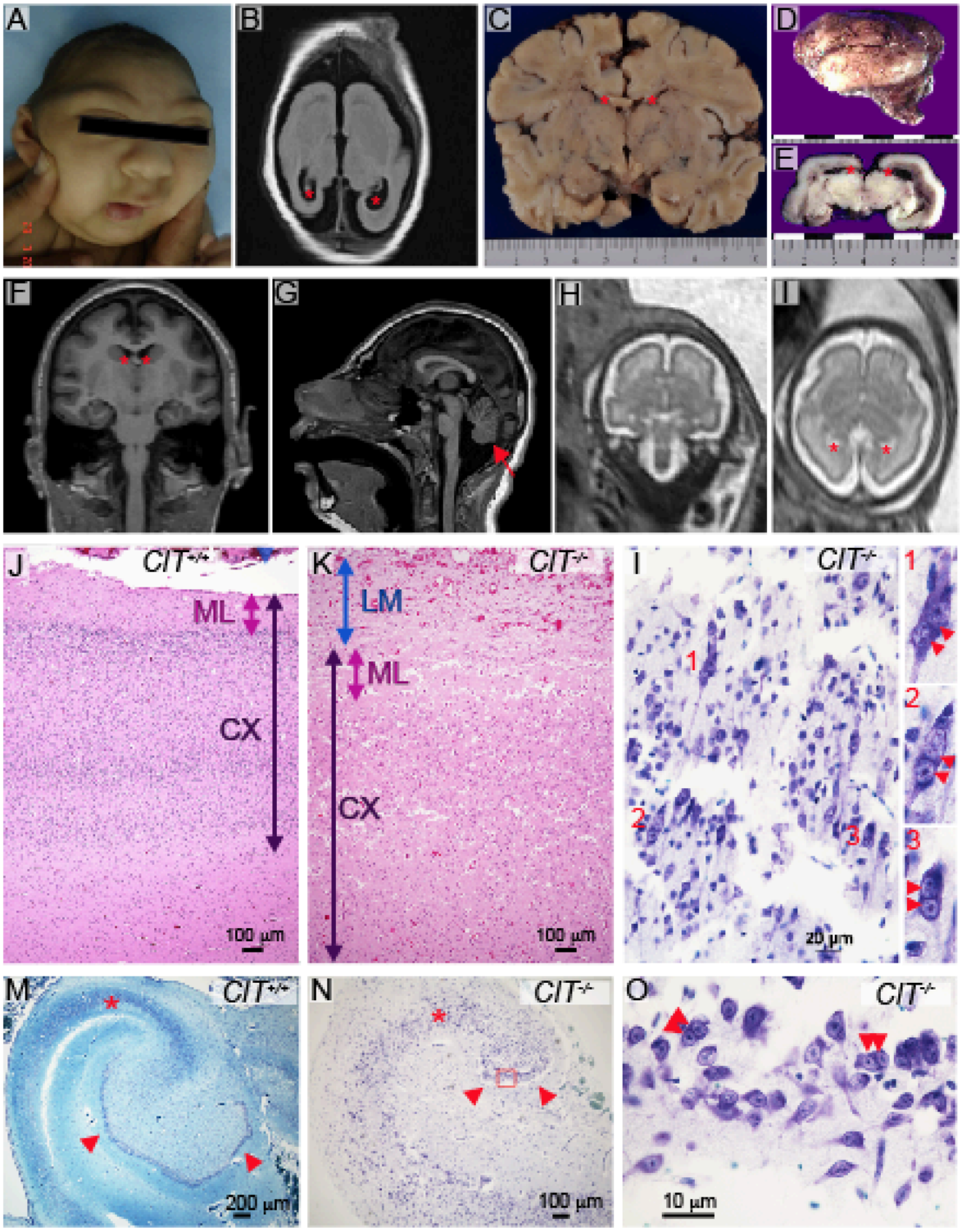

Structural and cellular neocortical phenotypes. (**A**) Proband A displays a microcephalic cranium, sloping forehead, wide nasal bridge and hypotelorism. (**B**) T2-weighted axial magnetic

resonance imaging (MRI) of Proband A at 3.5 months. Cerebral cortical size is markedly reduced with simplification of gyral folding and enlarged ventricles (red asterisks). (**C**) Coronal section of newborn control brain. Width is in centimeters (cm) and lateral ventricles marked by red asterisks. (**D**) Lateral view of lissencephalic newborn brain from Proband B (scale in cm). (**E**) Coronal section through mid-thalamus of Proband B brain showing enlarged lateral ventricles (red asterisks). (**F)** Coronal brain MRI of Proband C at 10 years of age showing microcephaly, simplified gyral pattern and enlarged ventricles (red asterisks). (**G**) Mid-sagittal MRI of Proband C showing sloping forehead, hypoplastic brainstem and cerebellum (red arrow) (**H**) Coronal and (**I**) axial fetal brain MRI of affected subject C:II:2 at 29 GWs. Reduced brain volume, gyrification and enlarged ventricles (red asterisks) were noted. (**J**) Control and (**K**) Proband B cerebral cortex stained with hematoxylin and eosin (H&E). Compared to control (j) leptomeninges (LM; blue arrow) are excessively thick and contiguous with molecular layer (ML; pink arrow) in proband (k). Cortex (CX; dark purple arrow) is thickened and cortical layering obscure when compared with control (j). (**L**) High magnification of Proband B cortex stained with Kluver-Barrera. Disorganized parenchyma includes many multinucleated neurons: inserts show detail of multinucleated (red double arrowheads) cells labeled 1,2,3. (**M-N**) Kluver-Barrera stained sections of control (m) and Proband B (n) temporal lobe. The proband hippocampus (n) is very small with hypoplastic pyramidal layer (red asterisk) and greatly reduced dentate gyrus (arrowheads). Image of normal control hippocampus (m) imaged at half the magnification to allow for comparison of overall structure of the hippocampus. (**O**) Detail of Proband B dentate gyrus (red box in H), showing binucleated granule cells (double arrowheads).

Figure 4.

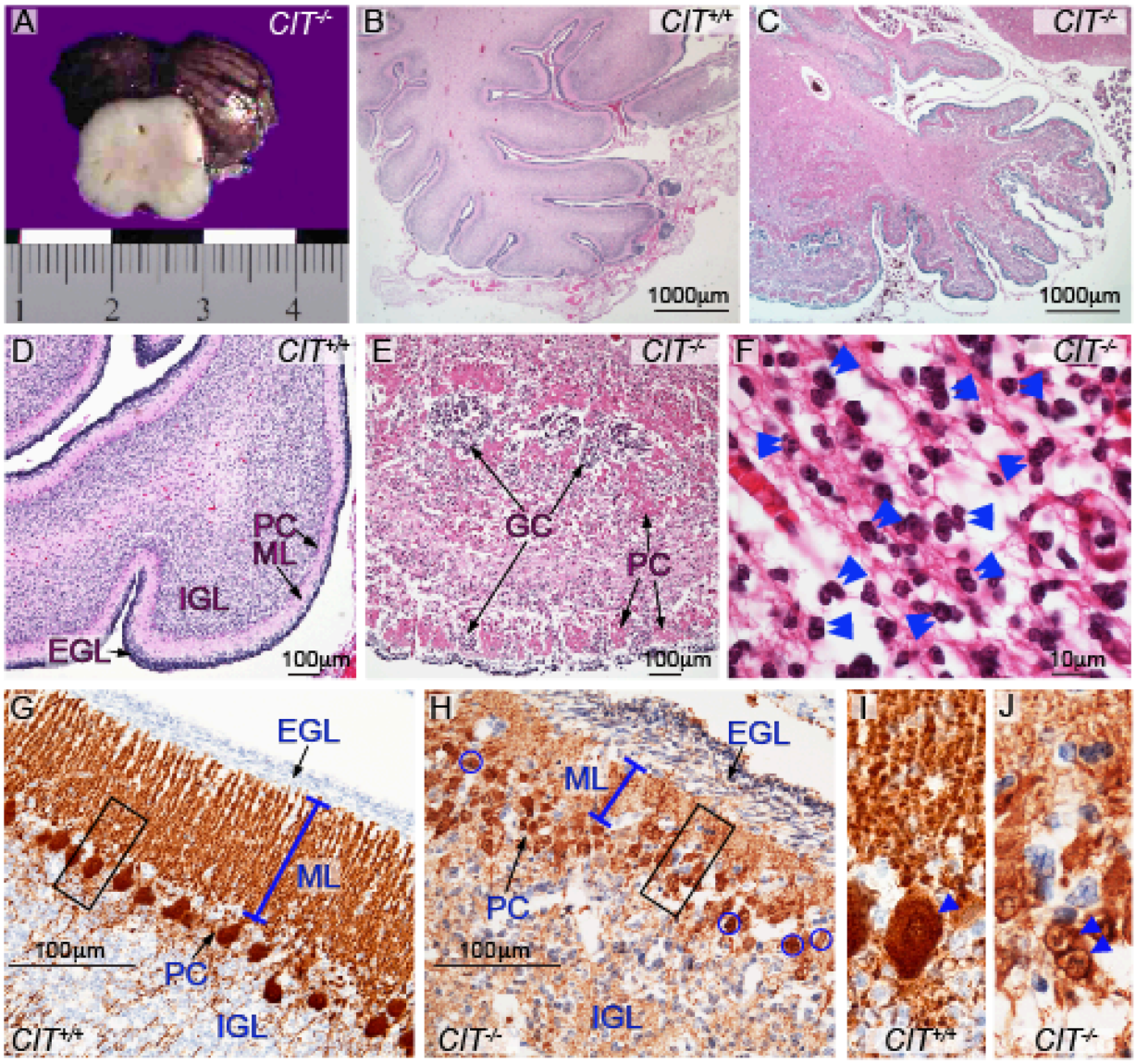

Structural and cellular cerebellar *CIT* phenotypes. (**A**) Section though Proband B midbrain with external view of hypoplastic cerebellum. (**B-F**) histologic sections of cerebellum, stained H&E. Cerebellar folia are poorly developed and the cortex disorganized in Proband B (c,e & h). Cerebellar lamination in Proband B is disrupted with clustered Purkinje cells (PC) interspersed with granule cells (GC) within fused folia (c, e) as compared to control cerebellum (b, d). (**F**) Many GC appear binucleated (double blue arrowheads). (**G-J**) Cerebellum immunostained for calbindin shows abnormally thick EGL, reduced ML (blue line) and multilayered collections of

small PCs (arrows) in Proband B (h), as compared with control (g). (**I-J**) Dashed boxes are enlarged to show binucleated PC (blue arrow heads) within a small soma in Proband B tissue (j) as compared to controls (i). EGL=external granule layer, IGL=internal granule layer, ML=molecular layer.